

---

# CUMULANT GAN

---

**Yannis Pantazis**

Institute of Applied and Computational Mathematics  
Foundation for Research & Technology - Hellas, Greece  
pantazis@iacm.forth.gr

**Dipjyoti Paul**

Computer Science Department  
University of Crete, Greece  
dipjyotipaul@csd.uoc.gr

**Michail Fasoulakis**

Institute of Computer Science  
Foundation for Research & Technology - Hellas, Greece  
mfasoul@ics.forth.gr

**Yannis Stylianou**

Computer Science Department  
University of Crete, Greece  
yannis@csd.uoc.gr

**Markos Katsoulakis**

Department of Mathematics and Statistics  
University of Massachusetts at Amherst, USA  
markos@math.umass.edu

## ABSTRACT

Despite the continuous improvements of Generative Adversarial Networks (GANs), stability and performance challenges still remain. In this work, we propose a novel loss function for GAN training aiming both for deeper theoretical understanding and improved performance of the underlying optimization problem. The new loss function is based on cumulant generating functions and relies on a recently-derived variational formula. We show that the corresponding optimization is equivalent to Rényi divergence minimization, thus offering a (partially) unified perspective of GAN losses: the Rényi family encompasses Kullback-Leibler divergence (KLD), reverse KLD, Hellinger distance and  $\chi^2$ -divergence. Wasserstein loss function is also included in the proposed cumulant GAN formulation. In terms of stability, we rigorously prove the convergence of the gradient descent algorithm for linear generator and linear discriminator for Gaussian distributions. Moreover, we numerically show that synthetic image generation trained on CIFAR-10 dataset is substantially improved in terms of inception score when weaker discriminators are considered.

## 1 Introduction

GANs [1] are powerful generative models capable of drawing new samples from an unknown distribution when only samples from that distribution are available. Their popularity stems from their ability to generate realistic samples from high-dimensional and complex distributions such as image collections [2, 3, 4, 5, 6, 7, 8], speech [9, 10, 11] and natural language text [12, 13] among other types of raw data.

A GAN is a two-player zero-sum game between a *discriminator* and a *generator*, both being strong neural networks. It is well-known that the training procedure of GANs often fails and several heuristics have been devised [14] to alleviate the difficulties of training. For instance, a recurring impediment with GAN training is the oscillatory behavior of the optimization algorithms due to the fact that the optimal solution is a saddle point of the loss function. Standard optimization algorithms such as stochastic gradient descent (SGD) may fail even for simple loss functions [15, 16].

Since their introduction, GANs have been also described as a tractable approach to minimize a divergence or a distance between the real data distribution and synthetic data distributions. Indeed, the original formulation of GAN [1] can be seen as the minimization of the *Shannon-Jensen divergence*, *f*-GAN [17] is a generalization of vanilla GAN where a variational lower bound for the *f*-divergence is minimized, *Wasserstein GAN* [18] which has been further improved in

[19] aims to minimize the Wasserstein distance increasing the stability of the training and similarly *Least-Squares GAN* [20] which minimizes a softened version of the Pearson  $\chi^2$ -divergence.

However, training might still be unstable and searching for the proper loss function, optimization algorithm and architecture can involve tedious trial-and-error. In this paper, we concentrate on the loss function selection. We propose a novel loss function based on cumulant generating functions with the resulting model referred as *Cumulant GAN*. By applying a recently-proposed variational representation formula [21], we show that Cumulant GAN is capable of interpolating between several well-known GAN formulations, thus offering a unified and flexible mathematical framework.

Our contributions are summarized as follows:

- We introduce *Cumulant GAN* with loss function based on cumulant generating functions of both real and synthetic data distributions.
- We interpret the novel and tunable loss function as the minimization of a divergence. Varying the hyperparameter values results in different divergences or probability metrics.
- We provide guaranteed convergence of the gradient descent algorithm in a special case with linear generator, linear discriminator and Gaussian distributions.
- We show improved performance on both synthetic and real datasets, especially, for weaker discriminators.

## 2 Background

Our results are a substantial generalization of the Wasserstein GAN by means of cumulant generating functions. These concepts are briefly discussed in this section.

### 2.1 Wasserstein GAN

Wasserstein GAN (WGAN) [18, 19] minimizes the Earth-Mover (Wasserstein-1) distance and primarily aims to stabilize the training procedure of GANs. Based on the Kantorovich-Rubinstein duality formula for Wasserstein distance, the loss function of WGAN can be written as

$$\min_G \max_{D \in \mathcal{D}} \mathbb{E}_{p_r}[D(x)] - \mathbb{E}_{p_g}[D(x)], \quad (1)$$

where  $p_r$  and  $p_g$  correspond to the real data distribution and the implicitly-defined model distribution, respectively. Namely,  $p_g$  denotes the distribution of  $G(z)$ , where  $G$  is the generator and  $z \sim p_z(z)$  is a random input vector often following a standard normal or uniform distribution.  $D(\cdot)$  is the discriminator (called critic in the WGAN setup) while  $\mathcal{D}$  is the function space of all 1-Lipschitz continuous functions. In WGAN, Lipschitz continuity is imposed by adding a (soft) regularization term on gradient values called Gradient Penalty (GP). It has been shown that GP regularization produces superior performance to weight clipping [19].

### 2.2 Cumulant Generating Functions

The cumulant generating function (CGF), also known as the log-moment generating function, is defined for a random variable with pdf  $p(x)$  as

$$\Lambda_{f,p}(\beta) = \log \mathbb{E}_p[e^{\beta f(x)}], \quad (2)$$

where  $f$  is a measurable function with respect to  $p$ . Typical CGFs are obtained when  $f(x) = x$ . CGF is a convex function with respect to  $\beta$  and it contains information for all moments of  $p$ . CGF also encodes the tail behavior of distributions and plays a key role in the theory of Large Deviations for the estimation of rare events [22]. A power series expansion of the CGF reveals that the lower order statistics dominate when  $|\beta| \ll 1$  while all statistics contribute to the CGF when  $|\beta| \gg 1$ . In statistical mechanics, CGF is the logarithm of the partition function while  $-\beta^{-1}\Lambda_{f,p}(-\beta)$  is called the Helmholtz free energy,  $\beta$  is interpreted as the inverse temperature and  $f$  as the Hamiltonian [23]. Furthermore, it is straightforward to show that  $\Lambda_{f,p}(0) = 0$  as well as  $\Lambda'_{f,p}(0) = \mathbb{E}_p[f(x)]$ , hence, the following limit for CGF holds

$$\lim_{\beta \rightarrow 0} \beta^{-1} \Lambda_{f,p}(\beta) = \mathbb{E}_p[f(x)] \quad (3)$$

We are now ready to introduce the new GAN model.

### 3 Cumulant GAN

#### 3.1 Definition

We define a novel GAN model by substituting the expectations in the loss function of WGAN with the respective CGFs. Thus, we propose to optimize the following minimax problem:

$$\begin{aligned} \min_G \max_{D \in \mathcal{D}} \{ & (-\beta)^{-1} \Lambda_{D, p_r}(-\beta) - \gamma^{-1} \Lambda_{D, p_g}(\gamma) \} \equiv \\ \min_G \max_{D \in \mathcal{D}} & \underbrace{-\beta^{-1} \log \mathbb{E}_{p_r}[e^{-\beta D(x)}] - \gamma^{-1} \log \mathbb{E}_{p_g}[e^{\gamma D(x)}]}_{=L(\beta, \gamma)}, \end{aligned} \quad (4)$$

where the hyper-parameters  $\beta$  and  $\gamma$  are two non-zero real numbers which control the learning dynamics as well as the optimal solution. Since the loss function is the difference of two CGFs, we call  $L(\beta, \gamma)$  in (4) the *cumulant loss function* and the respective generative model as *Cumulant GAN*. Throughout this paper, we assume the mild condition that both CGFs are finite for a neighborhood of  $(0, 0)$ , therefore, the cumulant loss is well-defined for  $|\beta| + |\gamma| < \epsilon$ , for some  $\epsilon > 0$ .

The definition of the loss function is extended on the axes and the origin of the  $(\beta, \gamma)$ -plane using the limit in (3). Hence, the cumulant loss function is defined for all the values of  $\beta$  and  $\gamma$  for which the new loss function is finite. It is straightforward to show that WGAN is a special case of cumulant GAN.

**Proposition 1.** *Let  $\mathcal{D}$  be the set of all 1-Lipschitz continuous functions. Then, cumulant GAN with  $(\beta, \gamma) = (0, 0)$  is equivalent to WGAN.*

*Proof.* The proposition is a consequence of the fact that

$$\lim_{\beta, \gamma \rightarrow 0} L(\beta, \gamma) = L(0, 0) = \mathbb{E}_{p_r}[D(x)] - \mathbb{E}_{p_g}[D(x)].$$

□

Next, we rigorously demonstrate that cumulant GAN can be seen as a unified and smooth interpolation between several well-known divergence minimization problems.

#### 3.2 KLD, Reverse KLD and Rényi Divergence as Special Cases

A major inconvenience of most GANs is their inability to interpret the loss function value and understand the properties of the obtained solution. Even when the stated goal is to minimize a divergence as in the original GAN and the  $f$ -GAN, the utilization of training tricks such as a non-saturating generators may result in the minimization of something completely different as it was recently observed [24]. In contrast, our proposed loss function can be interpreted for several choices of its hyper-parameters. Below there is a list of values for  $\beta$  and  $\gamma$  that result to interpretable loss functions. Indeed, several well-known divergences are recovered when the function space for the discriminator is the set of all measurable and bounded functions. In the following, we make the convention that a forward divergence or simply divergence is a divergence that uses the probability ratio,  $\frac{p_r}{p_g}$ , while a reverse divergence uses the reciprocal ratio.

**Theorem 1.** *Let  $\mathcal{D}$  be the set of all bounded and measurable functions. Then, the optimization of cumulant loss in (4) is equivalent to the minimization of*

- a. Kullback-Leibler divergence for  $(\beta, \gamma) = (0, 1)$ :

$$\min_G \max_{D \in \mathcal{D}} L(0, 1) \equiv \min_G D_{KL}(p_r || p_g).$$

- b. Reverse KLD for  $(\beta, \gamma) = (1, 0)$ :

$$\min_G \max_{D \in \mathcal{D}} L(1, 0) \equiv \min_G D_{KL}(p_g || p_r).$$

- c. Rényi divergence for  $(\beta, \gamma) = (\alpha, 1 - \alpha)$  with  $\alpha \neq 0$  and  $\alpha \neq 1$ :

$$\min_G \max_{D \in \mathcal{D}} L(\alpha, 1 - \alpha) \equiv \min_G \mathcal{R}_\alpha(p_g || p_r),$$

as well as for  $(\beta, \gamma) = (1 - \alpha, \alpha)$  with  $\alpha \neq 0$  and  $\alpha \neq 1$ :

$$\min_G \max_{D \in \mathcal{D}} L(1 - \alpha, \alpha) \equiv \min_G \mathcal{R}_\alpha(p_r || p_g),$$

where  $\mathcal{R}_\alpha(p||q)$  is the Rényi divergence defined by

$$\mathcal{R}_\alpha(p||q) = \frac{1}{\alpha(1-\alpha)} \log \mathbb{E}_q \left[ \left( \frac{p}{q} \right)^\alpha \right],$$

when  $p$  and  $q$  are absolutely continuous with respect to each other and  $\alpha > 0^1$ .

*Proof.* a. Using the definition of  $L(\beta, \gamma)$ , we have:

$$\begin{aligned} \max_{D \in \mathcal{D}} L(0, 1) &= \max_{D \in \mathcal{D}} \left\{ \mathbb{E}_{p_r}[D(x)] - \log \mathbb{E}_{p_g}[e^{D(x)}] \right\} \\ &= D_{KL}(p_r||p_g), \end{aligned}$$

where the last equation is the Donsker-Varadhan variational formula [25, 22].

b. Similarly,

$$\begin{aligned} \max_{D \in \mathcal{D}} L(1, 0) &= \max_{D \in \mathcal{D}} \left\{ -\log \mathbb{E}_{p_r}[e^{-D(x)}] - \mathbb{E}_{p_g}[D(x)] \right\} \\ &= \max_{D' = -D \in \mathcal{D}} \left\{ \mathbb{E}_{p_g}[D'(x)] - \log \mathbb{E}_{p_r}[e^{D'(x)}] \right\} \\ &= D_{KL}(p_g||p_r), \end{aligned}$$

where we applied again the Donsker-Varadhan variational formula.

c. Generalizing a. and b. we now have:

$$\begin{aligned} &\max_{D \in \mathcal{D}} L(\alpha, 1-\alpha) \\ &= \max_{D \in \mathcal{D}} \left\{ -\frac{1}{\alpha} \log \mathbb{E}_{p_r}[e^{-\alpha D(x)}] - \frac{1}{1-\alpha} \log \mathbb{E}_{p_g}[e^{(1-\alpha)D(x)}] \right\} \\ &= \max_{D' = -D \in \mathcal{D}} \left\{ \frac{1}{\alpha-1} \log \mathbb{E}_{p_g}[e^{(\alpha-1)D'(x)}] - \frac{1}{\alpha} \log \mathbb{E}_{p_r}[e^{\alpha D'(x)}] \right\} \\ &= \mathcal{R}_\alpha(p_g||p_r), \end{aligned}$$

where the last equation is an extension of the Donsker-Varadhan variational formula to Rényi divergence and was recently proved in (Theorem 5.4, [21]). For completeness, we provide a proof of the Rényi divergence variational representation in Appendix A.

The proof for the case  $L(1-\alpha, \alpha)$  is similar and agrees with the symmetry identity for the Rényi divergence,

$$\mathcal{R}_\alpha(p||q) = \mathcal{R}_{1-\alpha}(q||p).$$

□

The Rényi divergence,  $\mathcal{R}_\alpha$ , interpolates between KLD ( $\alpha \rightarrow 0$ ) and reverse KLD ( $\alpha \rightarrow 1$ ). Interestingly, there are additional special cases that belong to the family of Rényi divergences. The following corollary states some of them, while Figure 1 depicts schematically the obtained divergences and distances on the  $(\beta, \gamma)$ -plane.

**Corollary 1.** *Under the same assumption as in Theorem 1, the optimization of (4) is equivalent to the minimization of*

a. Hellinger distance for  $(\beta, \gamma) = (\frac{1}{2}, \frac{1}{2})$ :

$$\min_G \max_{D \in \mathcal{D}} L\left(\frac{1}{2}, \frac{1}{2}\right) \equiv \min_G -4 \log(1 - D_H^2(p_g, p_r)),$$

where  $D_H^2(p, q) = \frac{1}{2} \mathbb{E}_q \left[ \left( \left( \frac{p}{q} \right)^{1/2} - 1 \right)^2 \right]$  is the square of the Hellinger distance [26].

b.  $\chi^2$ -divergence for  $(\beta, \gamma) = (-1, 2)$ :

$$\min_G \max_{D \in \mathcal{D}} L(-1, 2) \equiv \min_G \frac{1}{2} \log(1 + \chi^2(p_r||p_g)),$$

---

<sup>1</sup>The definition is extended for  $\alpha < 0$  using the symmetry identity  $\mathcal{R}_\alpha(p||q) = \mathcal{R}_{1-\alpha}(q||p)$ .

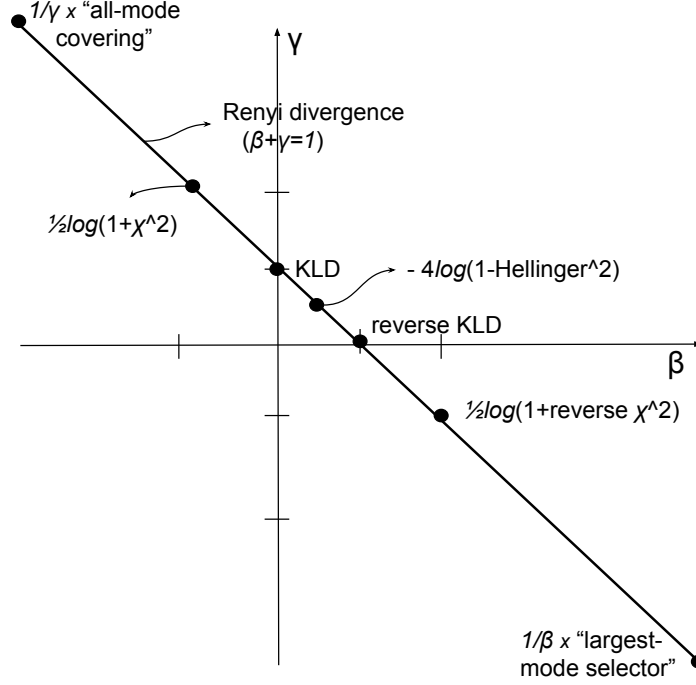


Figure 1: Special cases of *cumulant GAN*. Line defined by  $\beta + \gamma = 1$  has a point symmetry. The central point,  $(\frac{1}{2}, \frac{1}{2})$ , corresponds to the Hellinger distance. For each point,  $(\alpha, 1 - \alpha)$ , there is a symmetric one, i.e.,  $(1 - \alpha, \alpha)$ , which has the same distance from the symmetry point. The respective divergences have reciprocal probability ratios (e.g., KLD & reverse KLD,  $\chi^2$ -divergence & reverse  $\chi^2$ -divergence, etc.).

and reverse  $\chi^2$ -divergence for  $(\beta, \gamma) = (2, -1)$ :

$$\min_G \max_{D \in \mathcal{D}} L(2, -1) \equiv \min_G \frac{1}{2} \log (1 + \chi^2(p_g || p_r)),$$

where  $\chi^2(p || q) = \mathbb{E}_q \left[ \left( \frac{p}{q} - 1 \right)^2 \right]$  is the  $\chi^2$ -divergence<sup>2</sup> [26].

c. All-mode covering or worst-case regret in minimum description length principle [27] for  $(\beta, \gamma) = (\infty, -\infty)$ :

$$\min_G \lim_{\alpha \rightarrow \infty} \alpha \max_{D \in \mathcal{D}} L(\alpha, 1 - \alpha) \equiv \min_G \log \left( \operatorname{ess\,sup}_{x \in \operatorname{supp}(p_g)} \frac{p_g(x)}{p_r(x)} \right),$$

where  $\operatorname{ess\,sup}$  is the essential supremum of a function.

d. Largest-mode selector for  $(\beta, \gamma) = (-\infty, \infty)$ :

$$\min_G \lim_{\alpha \rightarrow \infty} \alpha \max_{D \in \mathcal{D}} L(1 - \alpha, \alpha) \equiv \min_G \log \left( \operatorname{ess\,sup}_{x \in \operatorname{supp}(p_r)} \frac{p_r(x)}{p_g(x)} \right).$$

<sup>2</sup>Forward  $\chi^2$ -divergence is often called Pearson  $\chi^2$ -divergence while the reverse  $\chi^2$ -divergence is often called Neyman  $\chi^2$ -divergence.

*Proof.* All cases a.-d. follow from Theorem 1.c as special instances of Rényi divergence:

$$\begin{aligned} R_{1/2}(p||q) &= -4 \log(1 - D_H^2(p, q)) \\ R_2(p||q) &= \frac{1}{2} \log(1 + \chi^2(p||q)) \\ R_{-1}(p||q) &= R_2(q||p) \\ \lim_{\alpha \rightarrow \infty} \alpha R_\alpha(p||q) &= \log \left( \operatorname{ess\,sup}_{x \in \operatorname{supp}(q)} \frac{p(x)}{q(x)} \right). \end{aligned}$$

We refer to [28, 29] and the references therein for detailed proofs.  $\square$

The flexibility of the two hyper-parameters is significant since they offer a simple recipe to remedy some of the most frequent issues of GAN training. For instance, KLD tends to cover all the modes of the real distribution while reverse KLD tends to select a subset of them [28, 29, 30, 31, 24] (see also Figure 3 for a benchmark example). Therefore, if mode collapse is observed during training, then, increasing  $\gamma$  with  $\beta = 1 - \gamma$  will push the generator towards generating a wider range of samples. In the other limit, more realistic samples (e.g. less blurry images) but with less variability will be generated when  $\beta$  is increased while  $\gamma = 1 - \beta$ .

**Remark 1.** *From a practical perspective, the boundedness condition required in the above theoretical findings can be easily enforced by considering a clipped discriminator with clipping factor  $M$ , i.e.,  $D_M(x) = M \tanh(\frac{D(x)}{M})$ . On the other hand, the set of all measurable functions is a very large class of functions and it is difficult to be represented by a neural network. However, when both probability densities  $p_r$  and  $p_g$  are continuous a relaxed function set—the set of all continuous and bounded functions, which can be approximated well in principle by an arbitrary neural network—can be substituted in the variational formula, and hence, in practice.*

### 3.3 Cumulant GAN as a Weighted Version of the SGD Algorithm

The parameter estimation for the cumulant GAN is performed using the SGD algorithm. Algorithm 1 presents the core part of SGD’s update steps where we exclude any regularization terms for clarity purposes. Namely,  $\eta$  and  $\theta$  are the parameters of the discriminator and the generator, respectively, while  $\lambda$  is the learning rate. Due to the fact that the proposed loss function is not the difference of two expected values, the order of application between differentiation and expectation approximation does matter. We choose to first approximate the expected values with the respective statistical averages as

$$\hat{L}_m(\beta, \gamma) = -\frac{1}{\beta} \log \sum_{i=1}^m e^{-\beta D(x_i)} - \frac{1}{\gamma} \log \sum_{i=1}^m e^{\gamma D(G(z_i))}. \quad (5)$$

Then, we apply the differentiation operator which results in a weighted version of SGD as shown in Algorithm 1. Interestingly, several recent papers [32, 31, 33, 34, 35] include a weighting perspective in their optimization approach.

---

#### Algorithm 1: Core of SGD Iteration

---

**Input:** data batch:  $\{x_i\}$ , noise batch:  $\{z_i\}$

**for**  $k$  steps **do**

$$\eta \leftarrow \eta + \lambda \left( \sum_{i=1}^m w_i^\beta \nabla_\eta D(x_i) - \sum_{i=1}^m w_i^\gamma \nabla_\eta D(G(z_i)) \right)$$

**end for**

$$\theta \leftarrow \theta + \lambda \left( \sum_{i=1}^m w_i^\gamma \nabla_\theta D(G(z_i)) \right)$$


---

The only difference between WGAN and cumulant GAN for the update steps is the weights  $w_i^\beta$  and  $w_i^\gamma$ . In WGAN, the weights are constant and equal to  $\frac{1}{m}$  while in cumulant GAN they are defined for any  $i = 1, \dots, m$  by

$$w_i^\beta = \frac{e^{-\beta D(x_i)}}{\sum_{j=1}^m e^{-\beta D(x_j)}}, \quad \text{and,} \quad w_i^\gamma = \frac{e^{\gamma D(G(z_i))}}{\sum_{j=1}^m e^{\gamma D(G(z_j))}}.$$

The weights redistribute the sample distributions based on the assessment of the current discriminator. Figure 2 demonstrates the change of the weight relative to uniform weights for  $\beta, \gamma > 0$ . The intuition behind the weighting mechanism is that samples that confuse the discriminator are more valuable for the training process than samples that are easily distinguished, thus, they should weigh more. Essentially, the discriminator is updated with samples produced by a better generator than the current one, as well as with more challenging real samples. Similarly, the generator is also updated using samples from a generator which is better than the current one. Overall, due to the use of the weights  $w_i^\beta, w_i^\gamma$  in Algorithm 1, both generator and discriminator updates will be more affected by synthetic samples that are more indistinguishable from the real ones.

Additionally, the update of the discriminator is performed  $k$  times more than the generator's update offering two important advantages. First, more iterations for the discriminator implies that it better distinguishes the real data from the generated ones, making the weighting perspective more valid. Second, it better approximates the optimal discriminator, thus, the theory presented in the previous section becomes more credible in practice.

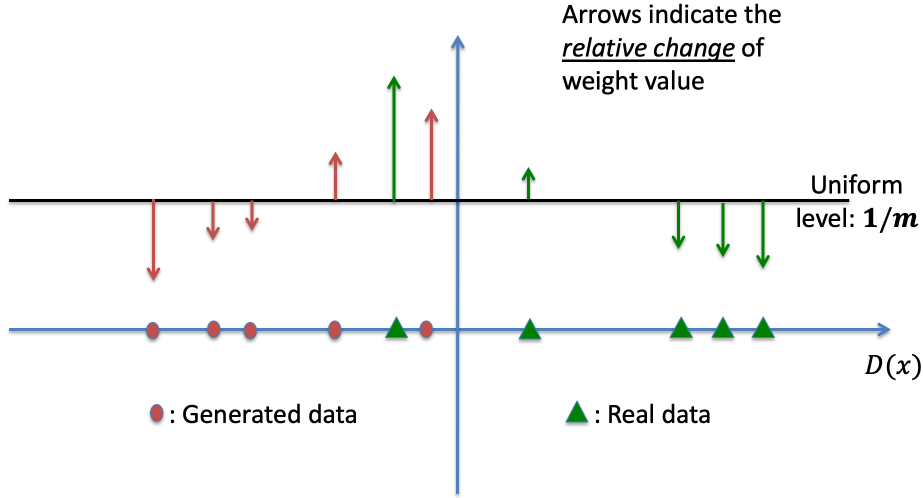


Figure 2: Interpretation of *cumulant GAN* as a weighted variation of SGD for  $\beta, \gamma > 0$ . Both real and generated samples for which the discriminator outputs a value closer to the decision boundary are assigned with larger weights because these are the samples which most probably confuse the discriminator.

**Remark 2.** *The Monte Carlo approximation resulting in (5) is biased. However, it has been shown that it is consistent [31], hence, the error due to the statistical approximation decreases as the size of minibatch increases. Bias correction gradients using moving averages have been utilized in [36] for the estimation of CGF. However, the modification of the loss function and the lack of an interpretation analogous to the weights  $w_i^\beta, w_i^\gamma$  are two key reasons to avoid adding any correction terms.*

### 3.4 Convergence Guarantees for Linear Discriminator

Let  $\mathcal{D}$  be the set of all linear functions (i.e.,  $D(x) = \eta^T x$  with  $\eta, x \in \mathbb{R}^d$ ) and assume that the real data follow a Gaussian distribution with mean value  $\mu \in \mathbb{R}^d$  and covariance matrix,  $I_d$ . The generator is defined by  $G(z) = z + \theta$ , where  $z$  is a standard  $d$ -dimensional Gaussian. The exact loss function for WGAN is

$$\min_{\theta} \max_{\eta} \eta^T (\mu - \theta),$$

while the respective exact cumulant loss function from (4) is

$$\min_{\theta} \max_{\eta} \eta^T (\mu - \theta) - \frac{\beta + \gamma}{2} \eta^T \eta.$$

It is known that the above WGAN loss function oscillates without converging to the optimum if gradient descent is used [15] and more sophisticated algorithms are required to guarantee convergence [16]. In contrast, the following theorem

demonstrates that the proposed cumulant loss function converges if gradient descent is used. Evidently, the use of the cumulant generating function transforms the optimization problem from just concave to a strongly concave problem for  $\eta$ . Next, without loss of generality we assume  $\gamma = 0$ .

**Theorem 2.** *The gradient descent method with learning rate  $\lambda$  converges exponentially fast to the (unique) Nash equilibrium with rate  $1 - \lambda\beta$  if  $\beta \in (0, \lambda^{-1})$ . Mathematically, for the  $t$ -th iteration of the gradient descent we have*

$$\|(\theta_t, \eta_t) - (\mu, 0)\|_2^2 \leq c(1 - \lambda\beta)^t, \quad (6)$$

where  $(\theta^*, \eta^*) = (\mu, 0)$  is the Nash equilibrium while  $c$  is a computable positive constant.

*Proof.* The update step of gradient descent for the cumulant loss is given by

$$\begin{aligned} \eta_{t+1} &= \eta_t + \lambda(\mu - \theta_t - \beta\eta_t), \\ \theta_{t+1} &= \theta_t + \lambda\eta_t. \end{aligned}$$

The proof is separated into two sub-cases depending on the value of  $\beta$ . We will consider first the case where  $0 < \beta \leq 1$  and then the reciprocal case where  $1 \leq \beta < \lambda^{-1}$ . This separation is needed because different auxiliary functionals are defined.

Case  $0 < \beta \leq 1$ : Define the energy function

$$E(\eta, \theta) = \eta^T \eta - \beta\eta^T(\mu - \theta) + (\mu - \theta)^T(\mu - \theta).$$

$E(\eta, \theta)$  is a second order polynomial for  $\eta$ ; it is straightforward to show that if  $0 < \beta \leq 1$  then  $E(\eta, \theta) \geq 0$  for all  $\eta$  and  $\theta$  and it is equal to 0 iff  $\eta = \eta^* = 0$  and  $\theta = \theta^* = \mu$ . Additionally, it generally holds that

$$\|(\theta, \eta) - (\mu, 0)\|_2^2 \leq 2E(\eta, \theta),$$

since  $2E(\eta, \theta) - \|(\theta, \eta) - (\mu, 0)\|_2^2 = \eta^T \eta - 2\beta\eta^T(\mu - \theta) + (\mu - \theta)^T(\mu - \theta) \geq 0$  for all  $0 < \beta \leq 1$ .

Next, we show that  $E(\eta_t, \theta_t)$  converges exponentially fast to 0. Since,  $E(\eta, \theta) = \sum_{i=1}^d \eta_i^2 - \beta\eta_i(\mu_i - \theta_i) + (\mu_i - \theta_i)^2$ , we can proceed with  $d = 1$  without sacrificing the generality of the proof. After some calculations, we obtain

$$\begin{aligned} E(\eta_{t+1}, \theta_{t+1}) &= (1 - \lambda\beta)E(\eta_t, \theta_t) \\ &\quad - \lambda^2[\eta_t^2 + \beta\eta_t(\mu - \theta_t) + (\mu - \theta_t)^2] \\ &\leq (1 - \lambda\beta)E(\eta_t, \theta_t), \end{aligned}$$

since  $\eta_t^2 + \beta\eta_t(\mu - \theta_t) + (\mu - \theta_t)^2 \geq 0$  for  $\beta \leq 1$ . The iterative application of this inequality yields

$$E(\eta_{t+1}, \theta_{t+1}) \leq (1 - \lambda\beta)^{t+1}E(\eta_0, \theta_0).$$

Combining the above inequalities we prove (6) with  $c = 2E(\eta_0, \theta_0)$ .

Case  $1 \leq \beta < \lambda^{-1}$ : Repeat the steps of the first case but this time for the modified energy function

$$\bar{E}(\eta, \theta) = \eta^T \eta - \beta^{-1}\eta^T(\mu - \theta) + (\mu - \theta)^T(\mu - \theta).$$

Here the positive constant is given by  $c = 2\bar{E}(\eta_0, \theta_0)$ . □

It is worth noting that the above theorem suggests a learning rate below but close to  $\frac{1}{\beta}$ . However, a statistical approximation of the exact cumulant loss is used in practice and the optimal learning rate is affected by the minibatch size, thus, it will necessarily have a smaller value.

**Remark 3.** *For the same discriminator and generator, the above theorem can be slightly generalized to the case where  $x \sim \mathcal{N}(\mu, \Sigma)$  and  $z \sim \mathcal{N}(0, \Sigma)$  with  $\Sigma$  being a positive-definite covariance matrix. The proof follows the same steps for the modified energy function  $E(\eta, \theta) = \eta^T \Sigma \eta - \beta\eta^T L(\mu - \theta) + (\mu - \theta)^T(\mu - \theta)$ , where  $L$  is the Cholesky decomposition of  $\Sigma$  (i.e.,  $\Sigma = LL^T$ ).*

### 3.5 Generalizations of the Cumulant Loss

The replacement of an expected value with the respective CGF need not be limited to Wasserstein GANs. It can be applied to other GAN loss functions resulting in new loss functions. As one example, we consider the vanilla GAN loss function, [1]

$$\min_G \max_D \mathbb{E}_{p_r}[\log(D(x))] + \mathbb{E}_{p_g}[\log(1 - D(x))].$$

The replacement of the expected values with the respective CGF results in the following optimization problem

$$\min_G \max_D -\frac{1}{\beta} \log(\mathbb{E}_{p_r}[D(x)^{-\beta}]) + \frac{1}{\gamma} \log(\mathbb{E}_{p_g}[(1 - D(x))^\gamma]).$$

Similar substitutions can be applied to the variational loss of  $f$ -GAN [17] or LSGAN [20]. Expected values in perceptual loss (i.e., deep feature matching) [37] and averaged cosine similarity loss (i.e., correlation loss) [38] can also be substituted with CGF. The theoretical and empirical ramifications of such substitutions are left as future work.



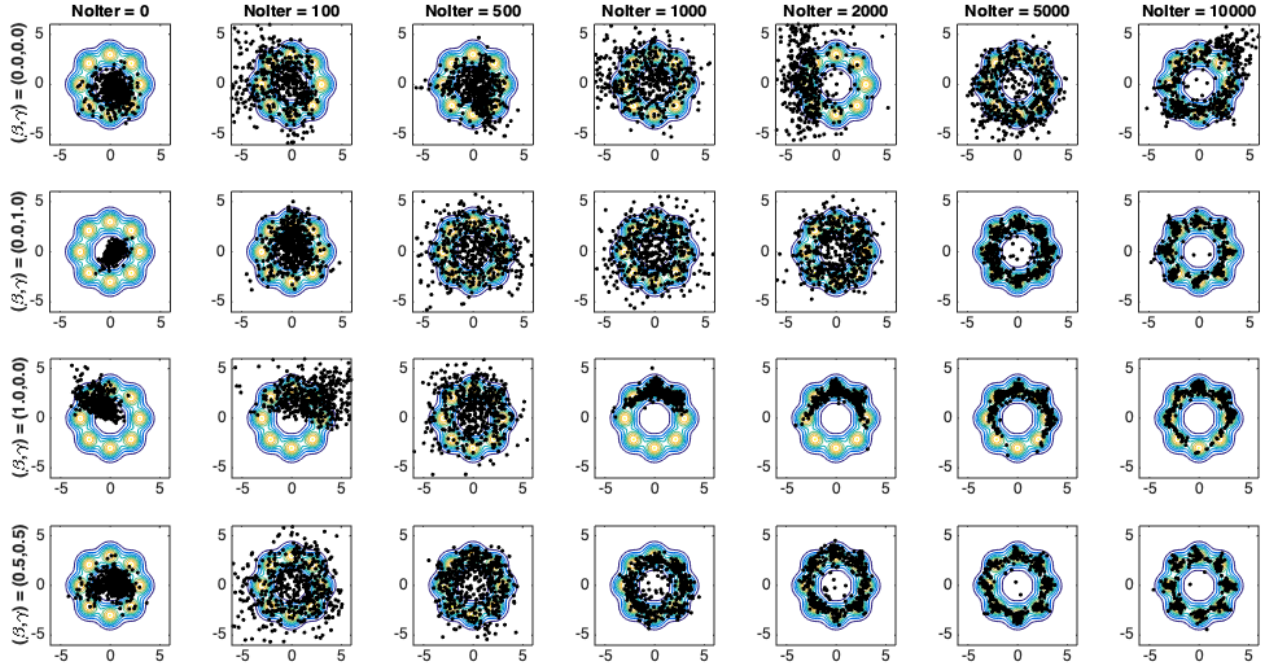


Figure 3: Generated samples using the Wasserstein distance using clipping (1st row), KL divergence (2nd row), reverse KLD (3rd row) and Hellinger distance (last row). A boundedness condition is not imposed on this example but it needs to be satisfied when the hyper-parameters take negative values.

## 4 Demonstrations

### 4.1 Traversing the $(\beta, \gamma)$ -plane: from Mode Covering to Mode Selection

As demonstrated in Section 3.2 and Figure 1, the optimization of cumulant GAN for the set of bounded and measurable functions and various hyper-parameter values is equivalent to the minimization of a divergence. It is well-known that different divergences result in fundamentally different behavior of the solution. For instance, KLD minimization tends to produce a distribution that covers all the modes while the reverse KLD tends to produce a distribution that is focused on a subset of the modes [28, 29, 30]. Taking the extreme cases, an all-mode covering is obtained as  $\beta \rightarrow -\infty$  while largest mode selection is observed at the other limit direction.

Our first example aims at highlighting the above characteristics of divergences and additionally to verify that the sub-optimal approximation of the function space of all bounded functions by a family of neural networks does not significantly affect the expected outcomes. Figure 3 presents generated samples for various values of the  $(\beta, \gamma)$  pair at different stages of the training process as quantified by the number of iterations (denoted by ‘NoIter’ in the Figure). The target distribution is a mixture of 8 equiprobable Gaussian random variables. Both discriminator and generator are neural networks with 2 hidden layers with 32 units each and ReLU as activation function. Input noise for the generator is an 8-dimensional standard Gaussian. In all cases, the discriminator is updated  $k = 5$  times followed by an update for the generator.

KLD minimization that corresponds to  $(\beta, \gamma) = (0, 1)$  (second row) tends to cover all modes while reverse KLD that corresponds to  $(\beta, \gamma) = (1, 0)$  (third row) tends to select a subset of them. This is particularly evident when the number of iterations is between 500 and 2000. Hellinger distance minimization (last row) produces samples with statistics that lie between KLD and reverse KLD minimization while Wasserstein distance minimization (first row) has a less controlled behavior. It is also noteworthy that reverse KLD was not able to fully cover all the modes after 10K iterations. This is not necessarily a drawback since the divergence of choice is primarily an application-specific decision. For instance, the lack of diversity might be sacrificed in image generation for the sake of sharpness of the synthetic images.

Finally, we remark that the plots in Figure 3, despite demonstrating a single run, are not cherry-picked. We have tested several architectures with more or fewer layers, as well as more or fewer units per layer, repeating each run several times, with qualitatively similar results.

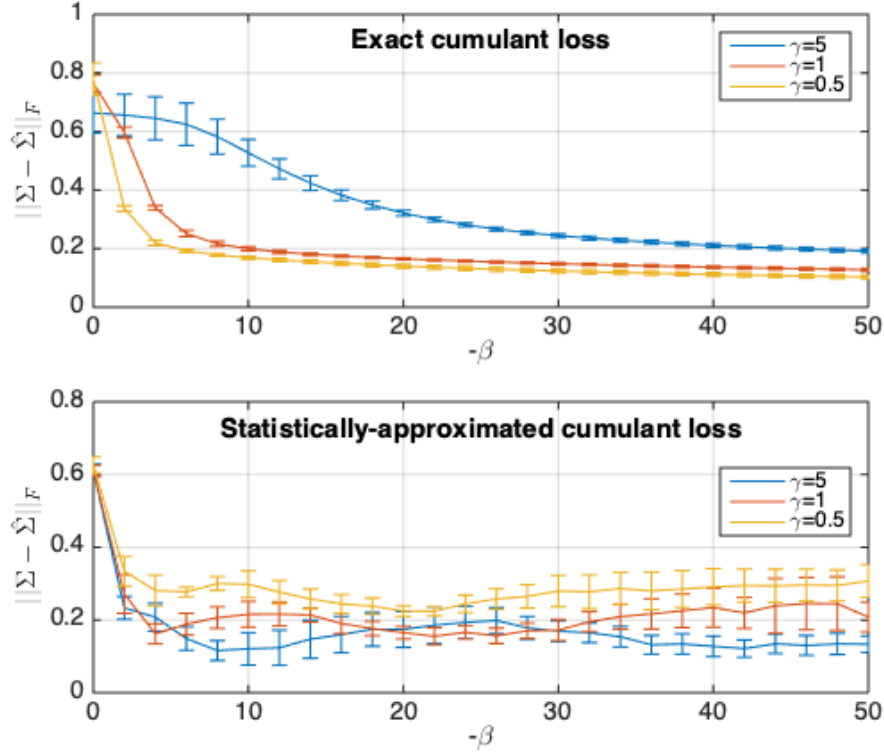


Figure 4: Covariance estimation error for the exact cumulant loss function (upper plot) and for the statistically-approximated cumulant loss function (lower plot).

## 4.2 Learning the Covariance Matrix of a Multivariate Gaussian

A CGF can uniquely determine a distribution and contains information on all moments. Therefore, the use of simple discriminators which may fail under the WGAN loss might be sufficient under the cumulant loss in order to successfully train the generator. In this section, we provide an example where the discriminator is a linear function and the target is to learn the second order statistic of a multivariate Gaussian distribution. Thus, the real data,  $x \in \mathbb{R}^d$ , follow a zero-mean Gaussian with covariance matrix  $\Sigma$ , the discriminator is given by  $D(x) = \eta^T x$  while the generator is given by  $G(z) = Az$  where  $A$  is a  $d \times k$  matrix and  $z$  is a standard  $k$ -dimensional Gaussian. The aim is to obtain a solution,  $\hat{\Sigma} = \hat{A}\hat{A}^T$ , close to the true covariance matrix.

The loss function of WGAN is

$$L(0, 0) = \eta^T \mathbb{E}_{p_r}[x] - \eta^T A \mathbb{E}_{p_z}[z] = 0,$$

Therefore, it is impossible here to learn the covariance matrix. On the other hand, the cumulant loss reads

$$L(\beta, \gamma) = -\frac{1}{2} \eta^T (\beta \Sigma + \gamma A A^T) \eta,$$

allowing the possibility of a  $(\beta, \gamma)$  pair that makes the Nash equilibrium non-trivially informative regarding the covariance matrix. Indeed, we calculated the best response diagrams for  $d = 1$  with fixed positive values of  $\gamma$  and inferred that suitable values are  $\beta \ll -1$ . Figure 4 presents the average error of the covariance matrix evaluated using the Frobenius norm as a function of  $\beta$ . The covariance is computed using either the above exact loss function (upper plot) or the statistical approximation of the cumulant loss along with stochastic gradient descent (lower plot) for three

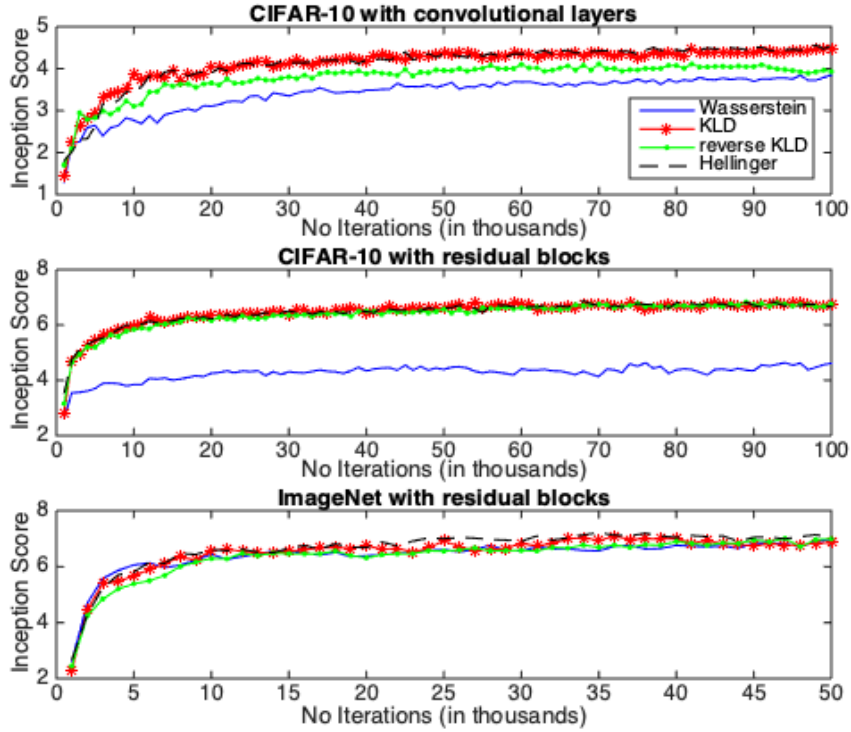


Figure 5: Inception score for CIFAR-10 (upper and middle plots) and ImageNet (lower plot) using a weaker discriminator relative to the generator (i.e., with less conv. layers or less residual blocks).

values of  $\gamma$ . We use 10K samples for the latter case, average over 10 iterations and a different covariance matrix is used at each iteration. The true covariance matrix is rescaled so that its Frobenius norm equals to 1. We observe that the covariance matrix is learned satisfactorily when the exact loss function is used for large negative values of  $\beta$ . When the approximated, yet realistic, loss is used, the error between the true and the estimated covariance matrices increases after a certain value of  $-\beta$  because tail statistics (requiring a large amount of samples) start to take control. Overall, the clear conclusion is that cumulant GAN is able to learn higher-order statistics and produce samples with the correct covariance structure despite the fact very simple discriminators were deployed.

### 4.3 Improved Image Generation in CIFAR-10 and ImageNet Datasets

A series of experiments have been conducted that demonstrate the effectiveness of cumulant GAN on standard CIFAR-10 [39] and ImageNet [40] datasets.

**CIFAR-10.** This is a well studied dataset of  $32 \times 32 \times 3$  RGB color images with 10 classes. The performance of trained GANs is tested on two architectures. The first corresponds to convolutional layers while the second to residual blocks. For the generator of the first architecture, we use one linear layer followed by three convolutional layers while the discriminator is a single convolutional layer followed by one linear layer. The generator for the second architecture has four residual blocks while the discriminator consists of two residual blocks (details in Appendix D). We deliberately choose a weaker discriminator to challenge the training procedure. We test four different hyper-parameter values that correspond to WGAN, KLD, reverse KLD and Hellinger divergences. In all cases, the same gradient penalty is added. The implementation of cumulant GAN is based on available open-source code<sup>3</sup>. Following the reference code, we train the models with the Adam optimizer.

Upper and middle plots in Figure 5 present the inception score for both architectures. The inception score is widely used to evaluate the visual quality of generated image samples [14]. We observe that all hyper-parameter choices for

<sup>3</sup>[https://github.com/igul222/improved\\_wgan\\_training](https://github.com/igul222/improved_wgan_training)

cumulant GAN outperform the baseline WGAN-GP. Results reveal that KLD minimization is preferred with a relative improvement of 17.5% for convolutional architecture and 48.9% for residual blocks over the baseline WGAN-GP; similar improvements were found for the Hellinger distance. Reverse KLD has 5.5% & 48.5% relative improvement for convolutional architecture and residual blocks, respectively. Evidently, each cumulant GAN version takes into consideration all moments of discriminator, i.e., all higher-order statistics and not just mean values, leading to better realization of the target data distribution. The samples generated by cumulant GAN also exhibit larger diversity and are visually better (Appendix E).

**ImageNet.** This large scale dataset consists of  $64 \times 64 \times 3$  color images with 1000 object classes. The large number of classes is challenging for GANs due to their tendency to underestimate the entropy in the distribution [14]. Even though improved performance can be potentially achieved by exploring a wider range of architectures, we choose to test the previous architecture that comprises of four residual blocks for the generator and two residual blocks for the discriminator. The lower plot of Figure 5 reveals similar performance in terms of inception score for baseline WGAN-GP and all variants of cumulant GAN. The observed differences in inception scores are statistically insignificant. By visual inspection of the generated images (Appendix E), we conclude that the generators learn some basic and contiguous shapes with natural color and texture. Nevertheless, cumulant GAN provides better images with object specifications that are clearly more realistic.

## 5 Conclusions and Future Directions

We proposed the cumulant GAN by establishing a novel loss function based on the CGF of the real and generated distributions. The use of CGFs allows for an inclusive characterization of the distributions' statistics, making it possible to partially remove complexity from the discriminator. Furthermore, cumulant GAN has the capacity to interpolate between a wide range of divergences and distances by simply changing the two hyper-parameter values  $(\beta, \gamma)$ , and thus offers a flexible and comprehensive mechanism to choose –possibly adaptively– which objective to minimize. Yet, most of the  $(\beta, \gamma)$  cumulant GAN plane remains *terra incognita* and we plan to explore its properties in the future. Additional future directions include the use of Rényi variational representations for other estimation and inference applications and the application of the proposed cumulant loss function beyond image generation applications.

## Acknowledgments

Yannis Pantazis acknowledges partial support by the project “Innovative Actions in Environmental Research and Development (PEnAn)” (MIS 5002358) funded by the Operational Programme "Competitiveness, Entrepreneurship and Innovation" (NSRF 2014-2020). Dipjyoti Paul has received for this work funding from the EU H2020 Research and Innovation Programme under the MSCA GA 67532 (the ENRICH network: [www.enrich-etn.eu](http://www.enrich-etn.eu)). Dr. Michail Fasoulakis is supported by the Stavros Niarchos-FORTH postdoc fellowship for the project ARCHERS. The research of Markos Katsoulakis was partially supported by the HDR-TRIPODS program of the National Science Foundation (NSF) under the grant CISE-1934846 and by the Air Force Office of Scientific Research (AFOSR) under the grant FA-9550-18-1-0214.

## References

- [1] I. J. Goodfellow, J. Pouget-Abadie, M. Mirza, B. Xu, D. Warde-Farley, S. Ozair, A. C. Courville, and Y. Bengio. Generative Adversarial Nets. In *Proceedings of the Annual Conference on Neural Information Processing Systems*, pages 2672–2680, 2014.
- [2] M. Mirza and S. Osindero. Conditional generative adversarial nets. *arXiv preprint arXiv:1411.1784*, 2014.
- [3] A. Radford, L. Metz, and S. Chintala. Unsupervised representation learning with deep convolutional generative adversarial networks. *arXiv preprint arXiv:1511.06434*, 2015.
- [4] Augustus Odena, Christopher Olah, and Jonathon Shlens. Conditional image synthesis with auxiliary classifier GANs. In *Proceedings of the International Conference on Machine Learning*, volume 70, pages 2642–2651, 2017.
- [5] Tero Karras, Timo Aila, Samuli Laine, and Jaakko Lehtinen. Progressive growing of GANs for improved quality, stability, and variation. In *Proceedings of the International Conference on Learning Representations*, 2018.
- [6] M. Brundage, S. Avin, J. Clark, H. Toner, P. Eckersley, B. Garfinkel, A. Dafoe, P. Scharre, T. Zeitzoff, B. Filar, et al. The malicious use of artificial intelligence: Forecasting, prevention, and mitigation. *arXiv preprint arXiv:1802.07228*, 2018.

- [7] Andrew Brock, Jeff Donahue, and Karen Simonyan. Large scale GAN training for high fidelity natural image synthesis. In *Proceedings of the International Conference on Learning Representations*, 2018.
- [8] Tero Karras, Samuli Laine, and Timo Aila. A style-based generator architecture for generative adversarial networks. In *Proceedings of the IEEE Conference on Computer Vision and Pattern Recognition*, pages 4401–4410, 2019.
- [9] Santiago Pascual, Antonio Bonafonte, and Joan Serrà. SEGAN: Speech enhancement generative adversarial network. In *Proceedings of the INTERSPEECH*, pages 3642–3646, 2017.
- [10] Y. Saito, S. Takamichi, and H. Saruwatari. Statistical parametric speech synthesis incorporating generative adversarial networks. *IEEE/ACM Transactions on Audio, Speech, and Language Processing*, 26(1):84–96, 2018.
- [11] Kundan Kumar, Rithesh Kumar, Thibault de Boissiere, Lucas Gestein, Wei Zhen Teoh, Jose Sotelo, Alexandre de Brébisson, Yoshua Bengio, and Aaron C Courville. Melgan: Generative adversarial networks for conditional waveform synthesis. In *Proceedings of the Advances in Neural Information Processing Systems*, pages 14881–14892, 2019.
- [12] T. Che, Y. Li, R. Zhang, R. D. Hjelm, W. Li, Y. Song, and Y. Bengio. Maximum-likelihood augmented discrete generative adversarial networks. *arXiv preprint arXiv:1702.07983*, 2017.
- [13] William Fedus, Ian Goodfellow, and Andrew M Dai. Maskgan: Better text generation via filling in the  $\_$ . In *Proceedings of the International Conference on Learning Representations*, 2018.
- [14] T. Salimans, I. Goodfellow, W. Zaremba, V. Cheung, A. Radford, and X. Chen. Improved techniques for training GANs. In *Proceedings of the Advances in Neural Information Processing Systems*, pages 2234–2242, 2016.
- [15] Panayotis Mertikopoulos, Christos Papadimitriou, and Georgios Piliouras. Cycles in adversarial regularized learning. In *Proceedings of the Twenty-Ninth Annual ACM-SIAM Symposium on Discrete Algorithms*, pages 2703–2717, 2018.
- [16] Constantinos Daskalakis, Andrew Ilyas, Vasilis Syrgkanis, and Haoyang Zeng. Training GANs with optimism. In *Proceedings of the International Conference on Learning Representations*, 2018.
- [17] S. Nowozin, B. Cseke, and R. Tomioka. f-GAN: Training generative neural samplers using variational divergence minimization. In *Proceedings of the Advances in Neural Information Processing Systems*, pages 271–279, 2016.
- [18] Martin Arjovsky, Soumith Chintala, and Léon Bottou. Wasserstein generative adversarial networks. In *Proceedings of the International Conference on Machine Learning*, pages 214–223, 2017.
- [19] I. Gulrajani, F. Ahmed, M. Arjovsky, V. Dumoulin, and A. C. Courville. Improved training of Wasserstein GANs. In *Proceedings of the Advances in Neural Information Processing Systems*, pages 5767–5777, 2017.
- [20] Xudong Mao, Qing Li, Haoran Xie, Raymond YK Lau, Zhen Wang, and Stephen Paul Smolley. Least squares generative adversarial networks. In *Proceedings of the IEEE International Conference on Computer Vision*, pages 2794–2802, 2017.
- [21] Jeremiah Birrell, Paul Dupuis, Markos A Katsoulakis, Luc Rey-Bellet, and Jie Wang. Distributional robustness and uncertainty quantification for rare events. *arXiv preprint arXiv:1911.09580*, 2019.
- [22] Paul Dupuis and Richard S Ellis. A weak convergence approach to the theory of large deviations. *John Wiley & Sons*, 902, 2011.
- [23] Tony Lelièvre, Mathias Rousset, and Gabriel Stoltz. Free energy computations: A mathematical perspective. *World Scientific*, 2010.
- [24] Matt Shannon. The divergences minimized by non-saturating GAN training, 2020.
- [25] Monroe D Donsker and SR Srinivasa Varadhan. Asymptotic evaluation of certain markov process expectations for large time. IV. *Communications on Pure and Applied Mathematics*, 36(2):183–212, 1983.
- [26] Alexandre B Tsybakov. Introduction to nonparametric estimation. *Springer Science & Business Media*, 2008.
- [27] Peter D Grünwald et al. The minimum description length principle. *MIT Press Books*, 1, 2007.
- [28] Tom Minka et al. Divergence measures and message passing. Technical report, Technical report, Microsoft Research, 2005.
- [29] Christopher M. Bishop. *Pattern Recognition and Machine Learning (Information Science and Statistics)*. Springer-Verlag, Berlin, Heidelberg, 2006.
- [30] JM Hernández-Lobato, Y Li, M Rowland, D Hernández-Lobato, TD Bui, and RE Turner. Black-box  $\alpha$ -divergence minimization. In *Proceedings of the International Conference on Machine Learning*, volume 48, pages 1511–1520, 2016.

- [31] Yingzhen Li and Richard E Turner. Rényi divergence variational inference. In *Proceedings of the Advances in Neural Information Processing Systems*, pages 1073–1081, 2016.
- [32] Yuri Burda, Roger Grosse, and Ruslan Salakhutdinov. Importance weighted autoencoders. In *Proceedings of the International Conference on Learning Representations*, 2016.
- [33] Zhiting Hu, Zichao Yang, Ruslan Salakhutdinov, and Eric P. Xing. On unifying deep generative models. In *Proceedings of the International Conference on Learning Representations*, 2018.
- [34] R Devon Hjelm, Athul Paul Jacob, Tong Che, Adam Trischler, Kyunghyun Cho, and Yoshua Bengio. Boundary-seeking generative adversarial networks. In *Proceedings of the International Conference on Learning Representations*, 2018.
- [35] Yannis Pantazis, Dipjyoti Paul, Michail Fasoulakis, and Yannis Stylianou. Training generative adversarial networks with weights. In *Proceedings of the European Signal Processing Conference (EUSIPCO)*, 2019.
- [36] Mohamed Ishmael Belghazi, Aristide Baratin, Sai Rajeshwar, Sherjil Ozair, Yoshua Bengio, Aaron Courville, and Devon Hjelm. Mutual information neural estimation. In *Proceedings of the International Conference on Machine Learning*, pages 531–540, 2018.
- [37] Richard Zhang, Phillip Isola, Alexei A Efros, Eli Shechtman, and Oliver Wang. The unreasonable effectiveness of deep features as a perceptual metric. In *Proceedings of the IEEE Conference on Computer Vision and Pattern Recognition*, pages 586–595, 2018.
- [38] Sergey Novoselov, Vadim Shchemelinin, Andrey Shulipa, Alexander Kozlov, and Ivan Kremnev. Triplet loss based cosine similarity metric learning for text-independent speaker recognition. In *Interspeech*, pages 2242–2246, 2018.
- [39] A. Krizhevsky and G. Hinton. Learning multiple layers of features from tiny images. Technical report, Citeseer, 2009.
- [40] J. Deng, W. Dong, R. Socher, L. Li, K. Li, and L. Fei-Fei. ImageNet: A large-scale hierarchical image database. In *IEEE Conference on Computer Vision and Pattern Recognition*, pages 248–255, 2009.
- [41] R. Atar, K. Chowdhary, and P. Dupuis. Robust bounds on risk-sensitive functionals via Rényi divergence. *SIAM/ASA Journal on Uncertainty Quantification*, 3(1):18–33, 2015.

## A A Variational Formula for Rényi Divergence

Similarly to the Donsker-Varadhan variational formula for the Kullback-Leibler divergence that can be obtained from the convex duality formula, we prove a variational formula for the Rényi divergence using the variational representation of exponential integrals also known as risk-sensitive functionals/observables.

**Theorem 3. (Variational Representation of Rényi Divergences)** *Let  $p$  and  $q$  be probability distributions. Then, the following formula holds:*

$$\mathcal{R}_\alpha(p||q) = \sup_{f \in C_b} \left\{ \frac{1}{\alpha - 1} \log \mathbb{E}_p[e^{(\alpha-1)f}] - \frac{1}{\alpha} \log \mathbb{E}_q[e^{\alpha f}] \right\}, \quad (7)$$

where  $C_b$  is the space of all bounded and measurable functions.

*Proof.* The authors in [41] proved that for all bounded and measurable functions  $f$  we have:

$$\frac{1}{\alpha - 1} \log \mathbb{E}_p[e^{(\alpha-1)f}] = \inf_q \left\{ \frac{1}{\alpha} \log \mathbb{E}_q[e^{\alpha f}] + \mathcal{R}_\alpha(p||q) \right\}.$$

Therefore, for any  $q$ ,

$$\begin{aligned} \frac{1}{\alpha - 1} \log \mathbb{E}_p[e^{(\alpha-1)f}] &\leq \frac{1}{\alpha} \log \mathbb{E}_q[e^{\alpha f}] + \mathcal{R}_\alpha(p||q) \\ \mathcal{R}_\alpha(p||q) &\geq \frac{1}{\alpha - 1} \log \mathbb{E}_p[e^{(\alpha-1)f}] - \frac{1}{\alpha} \log \mathbb{E}_q[e^{\alpha f}] \end{aligned}$$

For simplicity in the presentation, here we provide the proof based on the assumption that the function  $f = \log \frac{dp}{dq}$  is bounded and measurable. Based on the aforementioned assumption we have:

$$\begin{aligned} &\frac{1}{\alpha - 1} \log \mathbb{E}_p[e^{(\alpha-1) \log \frac{dp}{dq}}] - \frac{1}{\alpha} \log \mathbb{E}_q[e^{\alpha \log \frac{dp}{dq}}] \\ &= \frac{1}{\alpha - 1} \log \mathbb{E}_q[(\frac{dp}{dq})^\alpha] - \frac{1}{\alpha} \log \mathbb{E}_q[(\frac{dp}{dq})^\alpha] \\ &= \frac{1}{(\alpha - 1)\alpha} \log \mathbb{E}_q[(\frac{dp}{dq})^\alpha] \\ &= \mathcal{R}_\alpha(p||q) \end{aligned}$$

Therefore, the supremum is attained hence we proved (7). We refer to [21] for the complete and general proof.  $\square$

It is not hard to show that the variational formula for Rényi divergence reduces to the well-known Donsker-Varadhan variational formula for the Kullback-Leibler divergence, when  $\alpha \rightarrow 1$ , [21].

## B Concavity Property of Cumulant GAN

The concavity of the logarithmic function implies that

$$\beta^{-1} \Lambda_{f,p}(\beta) \geq \mathbb{E}_p[f(x)],$$

which is nothing else but Jensen's inequality. If additionally  $f$  is bounded, i.e., there is  $M > 0$  such that  $|f(x)| \leq M$  for all  $x$  then a stronger inequality is obtained due to the fact that the domain of the logarithm is also bounded. Indeed, logarithm is strongly concave with modulus equal to the infimum value of the domain. In our case, strongly Jensen's inequality deduces that

$$\beta^{-1} \Lambda_{f,p}(\beta) \geq \mathbb{E}_p[f(x)] - \beta e^{-\beta M} \text{Var}_p(f(x))$$

From Jensen's inequality (B), it is easy to show that for all  $\beta, \gamma \neq 0$

$$L(\beta, \gamma) \geq L(0, 0) = \mathbb{E}_{p_r}[D(x)] - \mathbb{E}_{p_g}[D(x)]$$

A stricter inequality called Jensen's inequality for strongly convex/concave functions can be obtained is the function  $D$  is bounded. Indeed, if  $|D(x)| < M$  for all  $x$  then the domain of the logarithmic function is also bounded leading to the stronger inequality

$$L(\beta, \gamma) \geq \mathbb{E}_{p_r}[D(x)] - \mathbb{E}_{p_g}[D(x)] - \beta e^{-\beta M} \text{Var}_{p_r}(D(x)) - \gamma e^{-\gamma M} \text{Var}_{p_g}(D(x)).$$

Generally speaking, strong concavity/convexity is a strengthening of the notion of concavity/convexity, and some properties of strongly concave/convex functions are just "stronger versions" of analogous properties of concave/convex functions.

## C Cumulant GAN Implementation

Next, we present the core part of the implementation of *cumulant GAN*.

```

fake_data = Generator()
disc_real = Discriminator(real_data)
disc_fake = Discriminator(fake_data)

def loss_function(disc_real, disc_fake, beta, gamma):

    max_val = tf.reduce_max((-beta) * disc_real)
    disc_cost_real =
        -(1.0/beta)*(tf.log(tf.reduce_mean(tf.exp((-beta)*disc_real-max_val)))+max_val)

    max_val = tf.reduce_max((gamma) * disc_fake)
    disc_cost_fake =
        (1.0/gamma)*(tf.log(tf.reduce_mean(tf.exp(gamma*disc_fake-max_val)))+max_val)
    gen_cost =
        -(1.0/gamma)*(tf.log(tf.reduce_mean(tf.exp(gamma*disc_fake-max_val)))+max_val)

    disc_cost = disc_cost_fake - disc_cost_real

    alpha = tf.random_uniform(
        shape=[64,1],
        minval=0., maxval=1.)

    differences = fake_data - real_data
    interpolates = real_data + (alpha*differences)
    gradients = tf.gradients(Discriminator(interpolates), [interpolates])[0]
    slopes = tf.sqrt(tf.reduce_sum(tf.square(gradients), reduction_indices=[1]))
    gradient_penalty = tf.reduce_mean((slopes-1.0)**2)
    disc_cost += 10*gradient_penalty

    gen_train_op = tf.train.AdamOptimizer(learning_rate=1e-4, beta1=0.,
        beta2=0.9).minimize(gen_cost,
        var_list=lib.params_with_name('Generator'),
        colocate_gradients_with_ops=True)

    disc_train_op = tf.train.AdamOptimizer(learning_rate=1e-4, beta1=0.,
        beta2=0.9).minimize(disc_cost,
        var_list=lib.params_with_name('Discriminator.'),
        colocate_gradients_with_ops=True)

    return gen_train_op, disc_train_op

```



## D Experimental Details

Here, we describe the experimental setup and architectural details for all the experiments presented in the paper. Three architectures have been used to compare the performance of four GAN losses: Wasserstein, Kullback-Leibler divergence (KLD), reverse KLD and Hellinger distance. The architectures whose successful training we demonstrate are described as follows: (i) convolutional layer for CIFAR-10 data, (ii) residual blocks for CIFAR-10 data (iii) residual blocks for ImageNet data. In the convolutional architecture, batch normalization is applied only for generator but not for discriminator. Whereas, we implemented layer normalization in both generator and discriminator. We used Adam as the optimizer with a learning rate of 0.0001. We trained the model for a total of 100,000 iterations on CIFAR-10 and 50,000 iterations on ImageNet, with a mini-batch of 128 and 64, respectively.

### D.1 CIFAR-10 Convolutional Architecture

Generator				
Layer	Kernel	Output shape	Stride	Activation function
Input $z$	-	128	-	-
Linear	-	$512 \times 4 \times 4$	-	-
Transposed convolution 1	$5 \times 5$	$256 \times 8 \times 8$	1	ReLU
Transposed convolution 2	$5 \times 5$	$128 \times 16 \times 16$	1	ReLU
Transposed convolution 3	$5 \times 5$	$3 \times 32 \times 32$	1	tanh
Discriminator				
Convolution	$5 \times 5$	$64 \times 32 \times 32$	4	Leaky ReLU
Linear	-	1	-	-

### D.2 CIFAR-10 Residual Architecture

Generator				
Layer	Kernel	Output shape	Stride	Activation function
Input $z$	-	128	-	-
Linear	-	$512 \times 2 \times 2$	-	-
Residual block 1	$3 \times 3$	$512 \times 4 \times 4$	1	ReLU
Residual block 2	$3 \times 3$	$256 \times 8 \times 8$	1	ReLU
Residual block 3	$3 \times 3$	$128 \times 16 \times 16$	1	ReLU
Residual block 4	$3 \times 3$	$64 \times 32 \times 32$	1	ReLU
Convolution	$3 \times 3$	$3 \times 32 \times 32$	1	tanh
Discriminator				
Convolution	$3 \times 3$	$64 \times 32 \times 32$	1	-
Residual block 1	$3 \times 3$	$128 \times 16 \times 16$	1	ReLU
Residual block 2	$3 \times 3$	$128 \times 8 \times 8$	1	ReLU
Linear	-	1	-	-

### D.3 ImageNet Residual Architecture

Generator				
Layer	Kernel	Output shape	Stride	Activation function
Input $z$	-	128	-	-
Linear	-	$512 \times 4 \times 4$	-	-
Residual block 1	$3 \times 3$	$512 \times 8 \times 8$	1	ReLU
Residual block 2	$3 \times 3$	$256 \times 16 \times 16$	1	ReLU
Residual block 3	$3 \times 3$	$128 \times 32 \times 32$	1	ReLU
Residual block 4	$3 \times 3$	$64 \times 64 \times 64$	1	ReLU
Convolution	$3 \times 3$	$3 \times 64 \times 64$	1	tanh
Discriminator				
Convolution	$3 \times 3$	$64 \times 64 \times 64$	1	-
Residual block 1	$3 \times 3$	$64 \times 32 \times 32$	1	ReLU
Residual block 2	$3 \times 3$	$128 \times 16 \times 16$	1	ReLU
Linear	-	1	-	-

## E Generated Images

In this section, generated samples from all the trained models are presented. We remark that all models are trained with GP regularization.

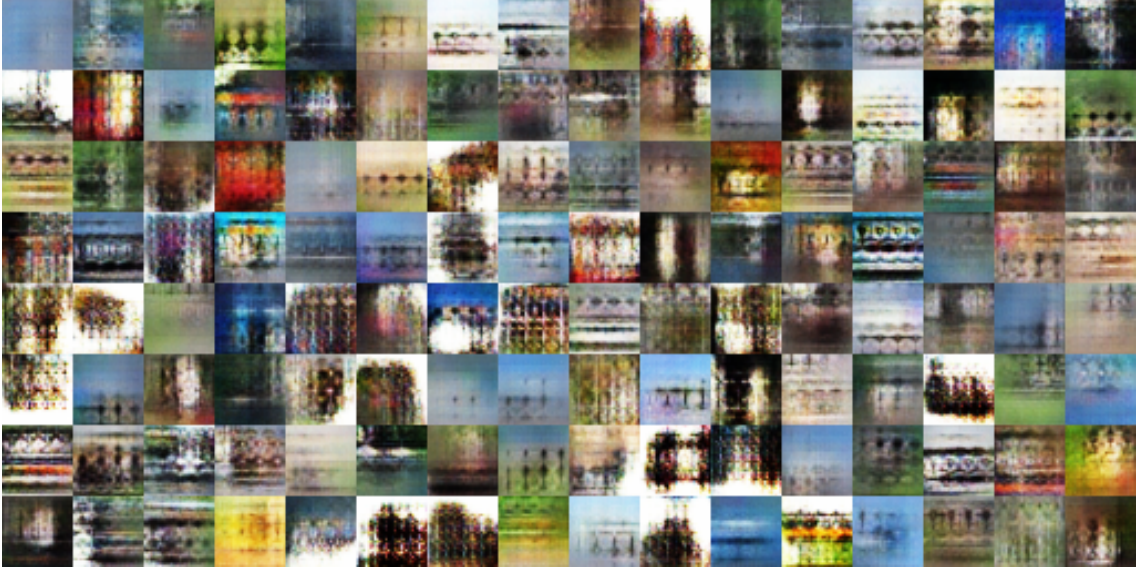


Figure 6: WGAN: Samples of CIFAR-10 from generator and discriminator trained with convolutional networks.

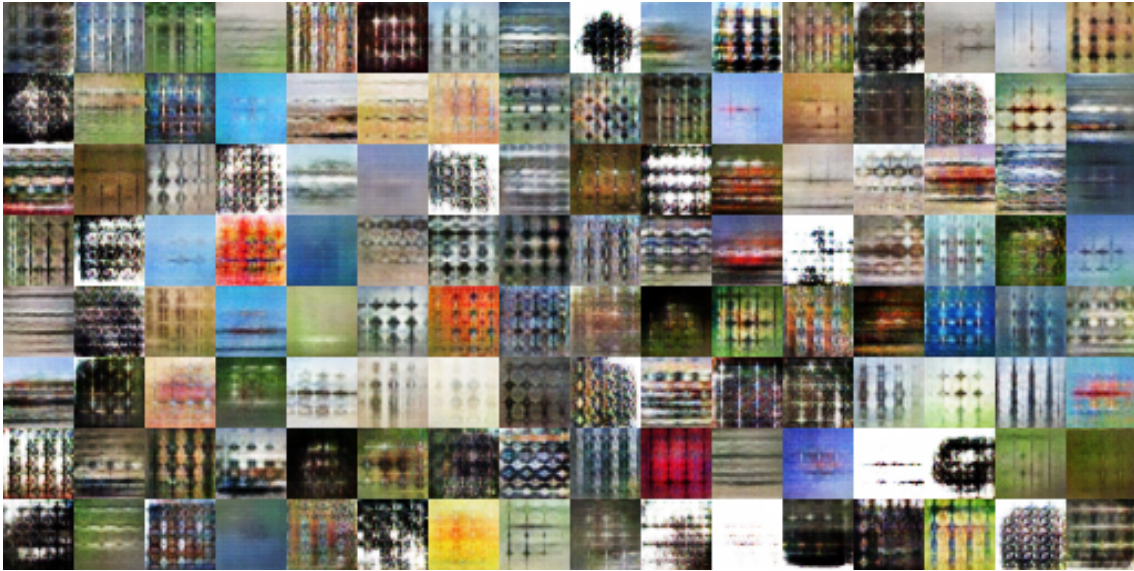


Figure 7: KLD: Samples of CIFAR-10 from generator and discriminator trained with convolutional networks.



Figure 8: Reverse KLD: Samples of CIFAR-10 from generator and discriminator trained with convolutional networks.



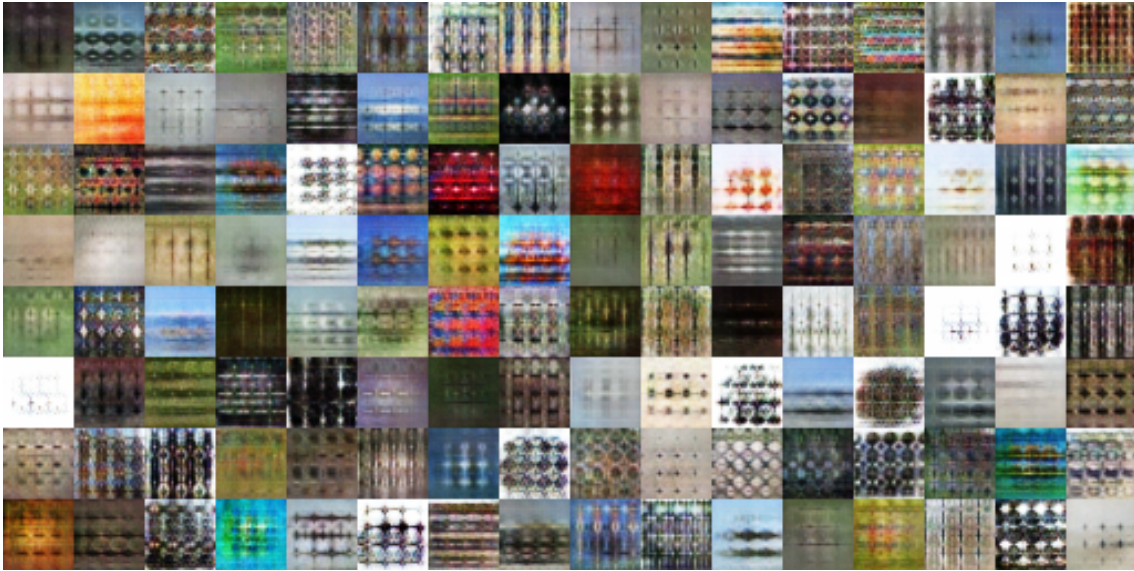


Figure 9: Hellinger: Samples of CIFAR-10 from generator and discriminator trained with convolutional networks.

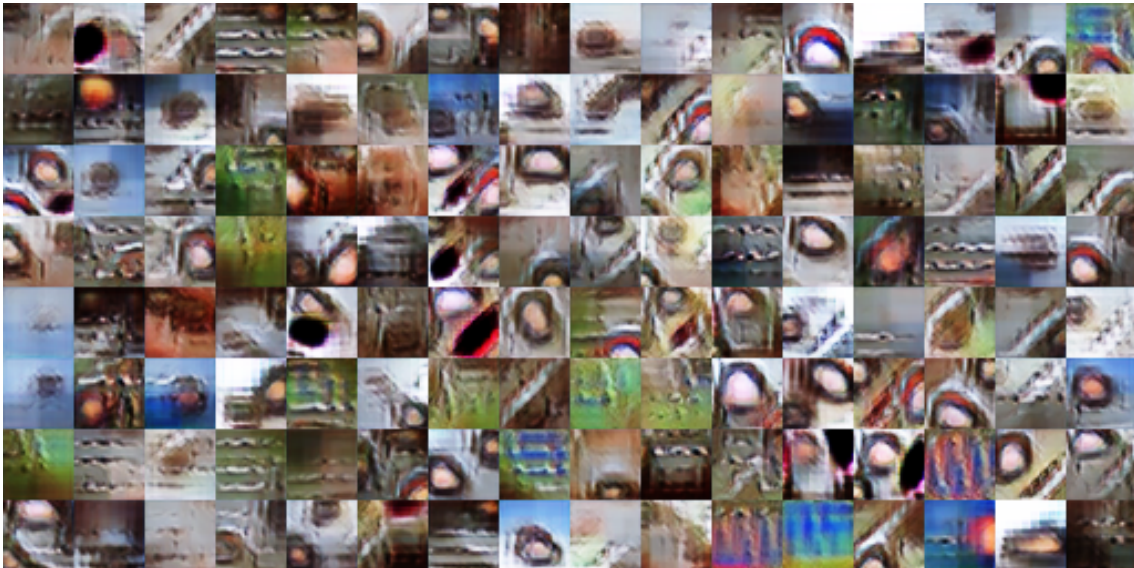


Figure 10: WGAN: Samples of CIFAR-10 from generator and discriminator trained with residual networks.



Figure 11: KLD: Samples of CIFAR-10 from generator and discriminator trained with residual networks.



Figure 12: Reverse KLD: Samples of CIFAR-10 from generator and discriminator trained with residual networks.



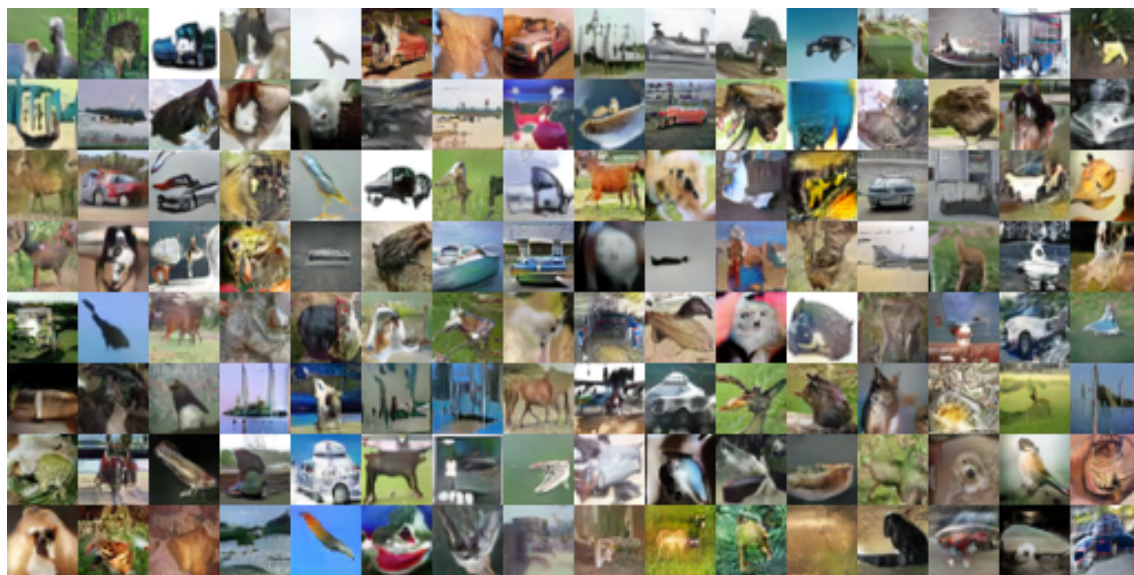


Figure 13: Hellinger: Samples of CIFAR-10 from generator and discriminator trained with residual networks.

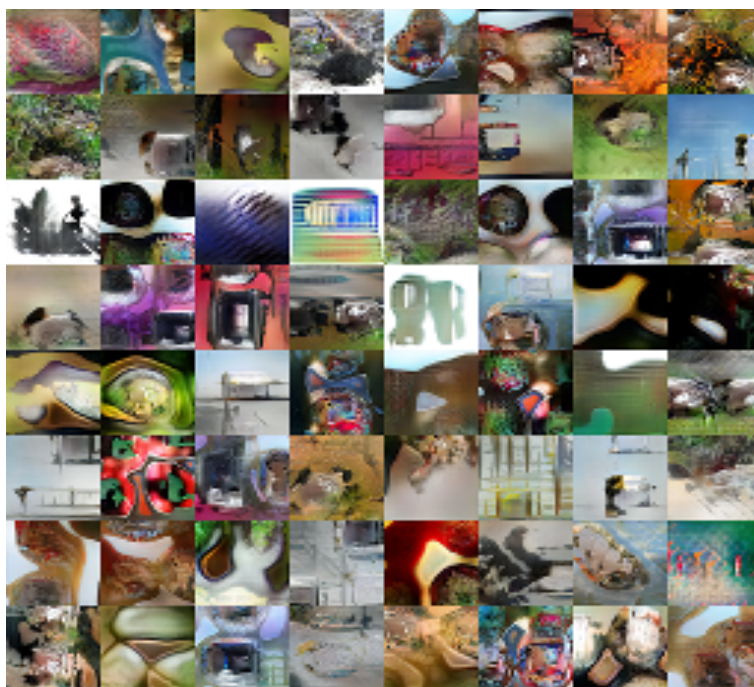


Figure 14: WGAN: Samples of ImageNet from generator and discriminator trained with residual networks.



Figure 15: KLD: Samples of ImageNet from generator and discriminator trained with residual networks.



Figure 16: Reverse KLD: Samples of ImageNet from generator and discriminator trained with residual networks.

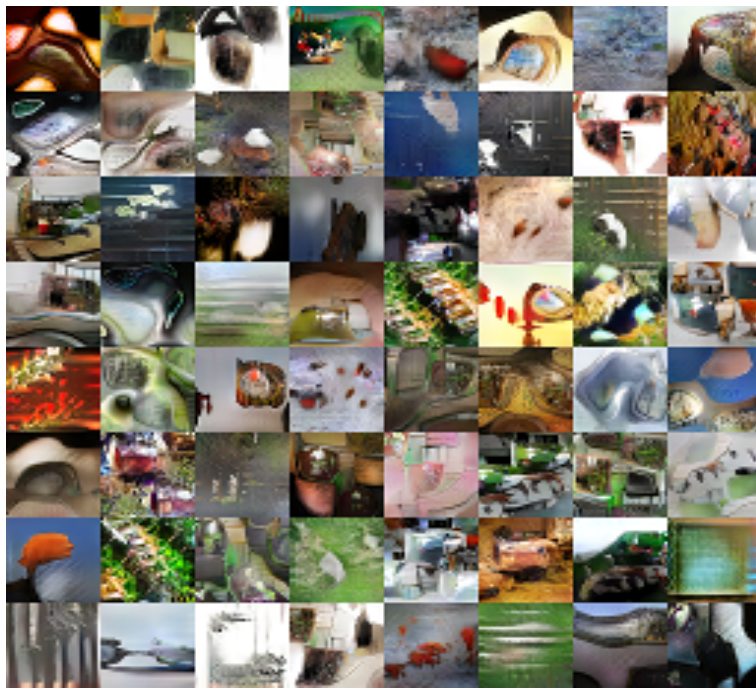


Figure 17: Hellinger: Samples of ImageNet from generator and discriminator trained with residual networks.